APRIL 1978

PPPL-1438
UC-20f

RECENT RESULTS FROM THE PLT TOKAMAK

BY

V. ARUNASALAM, C. BARNES, K. BOL, D. BOYD, K. BRAU, N. BRETZ, M. BRUSATI, S. COHEN, S. DAVIS, D. DIMOCK, F. DYLLA, D. EAMES, P. EFTHIMION, H. EUBANK, H. FURTH, R. GOLDSTON, R. HAWRYLUK, K. HILL, E. HINNOV, R. HORTON, J. HOSEA, H. HSUAN, D. IGNAT, F. JOBES, D. JOHNSON, M. MATTIOLI, E. MAZZUCATO, E. MESERVEY, P. MORIETTE, N. SAUTHOFF, J. SCHIVELL, G. SCHMIDT, R. SMITH, F. STAUFFER, W. STODIEK, J. STRACHAN, S. SUCKEWER, AND S. VON GOELER

PLASMA PHYSICS LABORATORY

PRINCETON UNIVERSITY
PRINCETON, NEW JERSEY

This work was supported by the U. S. Department of Energy Contract No. EY-76-C-02-3073. Reproduction, translation, publication, use and disposal, in whole or in part, by or for the United States Government is permitted.

Recent Results From The PLT Tokamak

V. Arunsalam, C. Barnes, K. Bol, D. Boyd***, K. Brau, N. Bretz, M. Brusati, S. Cohen, S. Davis, D. Dimock, F. Dylla, D. Eames, P. Efthimion, H. Eubank, H. Furth, P. Goldston, R. Hawryluk, K. Hill**, E. Hinnov, R. Horton, J. Hosea, H. Hsuan, D. Ignat, F. Jobes, D. Johnson, M. Mattioli*, E. Mazzucato, E. Meservey, P. Moriette*, N. Sauthoff, J. Schivell, G. Schmidt, R. Smith, F. Stauffer***, W. Stodiek, J. Strachan, S. Suckewer, S. von Goeler

Plasma Physics Laboratory, Princeton University
Princeton, New Jersey 08540

As reported at the Berchtesgaden meeting[1], the optimum plasma parameters during the initial phase of PLT operation were obtained by an empirical approach either in helium gas or in hydrogen gas with appreciable oxygen content. The second operating period has mainly been devoted to an investigation of this observation, and to an effort to vary, and especially to lower, the effective ion charge, Z, with a goal of obtaining stable discharges at high plasma densities. The third phase, supplementary heating with neutral beams, is beginning. This paper reports some of the results of the second phase.

The main result has been the recognition of the importance of radiation in the power balance. In smaller tokamaks, the energy confinement was mostly determined by plasma transport. In PLT, although transport is important, even in the central core of the plasma, power loss by radiation is often equally important. This reflects the fact that as devices are made larger, the ohmic power input density decreases and the

*On leave from Fontenay aux Roses (France).
**On leave from Oak Ridge National Laboratory.
***University of Maryland.

confinement due to plasma transport improves, and so volume effects like radiation will gain importance.

In Section I, we discuss impurity behavior, specifically the control of oxygen by discharge cleaning and the identification and quantitative measurement of tungsten radiation. In Section II, we compare the main types of PLT discharges, classified by tungsten content and MHD instability properties. In Section III, we discuss plasma confinement.

I. Impurity Behavior

A. Low Z Impurities - The second phase of PLT operation began with an effort to remove oxygen (the domiant low-Z impurity) from the discharge by low temperature discharge cleaning in hydrogen (TDC). It has been shown by Taylor[2] that TDC removes oxygen better than higher temperature discharges (Figure 1). The method is to raise the hydrogen pressure until the ohmic heating current is throttled from ~50 kA, to ~5 kA, the exact level being adjusted so as to maximize the pressure of water vapor at the pumps. Carbon is removed efficiently by either method, chiefly as methane. Table I illustrates the reduction of the relative oxygen and carbon concentration effected by the TDC method.

B. High Z Impurities: Tungsten - The primary effect of diminished light impurity concentration was an increase in radiation from the plasma core, sufficient to cause collapse of the electron temperature (Figure 2). Careful investigation[3] of iron, chromium and nickel (wall material) shows that their contribution to the power loss is not important; no evidence of an accumulation of iron in the center of the discharge was detected. Most of this radiation is attributable to tungsten, the limiter material and much effort has been devoted to a quantitative evaluation of the effect of tungsten.

In experiments at NRL[4] and Oak Ridge[5], strong bands of tungsten lines around 50 Å have been discovered which are believed to be $\Delta n=0$ transitions (4d-4f)(4p-4d)(4s-4p) from the ionization states W XVIII (ionization potential 420 eV) to W XLVI (ionization potential ~2400 eV).[6] Also, computer calculations of radiative power have been performed with the average ion model[7] which predict unexpectedly high emissivities.

Experimentally, the radiation has been investigated with a grazing incidence VUV spectrometer and with unshielded surface barrier diodes (USX-detectors). A VUV spectrum is shown in Figure 3. There are three bands of radiation, centered around 33, 50, and 59 Å, with the intensity in the ratio 3:5:2, each consisting of many overlapping lines. The broader band ($0.1<h\nu<1$ keV) USX-detector data are in close agreement with the VUV results. These diagnostics make possible relatively exact measurements of the total intensity of the tungsten radiation.

II. Discharge Types

During the first PLT phase, discharges were classified by certain MHD instability patterns: m=1 "sawtooth" discharges, "large m=2," "small m=2," etc. During the second phase, the concentration of tungsten became a classifying parameter of equal importance. The control of tungsten concentration is thus a major consideration in selecting operation conditions. In this regard, measurements of both ion and electron temperatures at the plasma edge have confirmed the view that there is positive correlation between edge temperature and tungsten concentration. However, it is clear that edge temperatures and MHD instabilities are coupled through changes in current profile, and the relative importance of each has not yet been sorted out. The mechanism for tungsten injection also remains unclear: Sufficient amounts could be released either by sputtering from the limiter by highly stripped oxygen ions accelerated in the sheath, or by unipolar arcs on the limiter.[8] Arc Tracks, in fact, can be seen on the limiter.

Table 2 compares five different discharge regimes which differ in the way the plasma edge was cooled, but with similar currents and toroidal fields (I_p = 400-500 kA, B_T = 30-35 kG). These are discussed in more detail below.

A. Discharges With Hollow Temperature Profiles - (Type I) Hollow temperature profiles develop reproducibly at low filling pressures after thorough discharge cleaning with TDC. (They were sometimes observed before TDC was applied.) The time development of the electron temperature is shown in Figure 4. The transition from a peaked to a hollow profile at time t=150 ms is typical although it is sometimes observed that the profile can stay hollow throughout the discharge, or that a minor disruption can fill in the hole. Due to the small current ($\propto T_e^{3/2}$)

in the central region, the central ohmic heating power input is smaller not only than the total radiated power, seen by the bolometer, but also smaller than the tungsten radiation alone (Table 2). The radiation is therefore sufficient to maintain the hollow profile. Actually, heat must be transported into the hollow region to make up the difference between radiation loss and power input. The transition from the peaked to the hollow profile is being analysed in terms of the thermal instability[9], with only partially satisfactory results. From the data during the peaked and the hollow phases, an empirical value for the heat conductivity is derived which is about the same for both phases. The calculated heat conductivity is so large that it inhibits the formation of the hole. Either a lowering of the heat conductivity, possibly locally during the transition period or an enhanced tungsten concentration in the center has to be assumed to allow the mechanism of Reference 9 to work. These results are, however, preliminary.

Hollow discharges tend to turn into peaked m=2 discharges (Type II) after some time of operation, often going through a period when discharges are intermittently hollow or peaked. In the Type II discharges (Figure 5) the central tungsten radiation is often stronger than in hollow discharges. The initial level, however, is low and rises later. Also, the oxygen content is usually somewhat higher. The main discharges in PLT apparently allow oxygen to build back up on the walls instead of removing it as the low-temperature discharges do; this gradually leads to transition from hollow to peaked discharges.

B. Programming of the Flow of Neutral Gas - With careful programming of the flow of neutral gas, the tungsten influx can be minimized. In practice, this means a high enough initial pressure to prevent too broad a current channel, and as much gas fed in during the discharge as possible while avoiding disruptions. The resulting discharges (Type III) have higher density, less tungsten radiation (Figure 6), higher electron and ion temperatures, and may exhibit sawteeth oscillations associated with the m=1 tearing mode.

In helium, gas programming is especially successful, and the central plasma density can be increased to $1.5 \times 10^{14}\ cm^{-3}$. We have therefore grouped these discharges in a separate column in Table 2 (Type IV). These discharges have the best confinement. The tungsten radiation level is very much reduced. In hydrogen, the initial tungsten level is about the same as in helium, but it has not been possible to keep it low during the later stages (Figure 6). This is probably a primary reason why the results in helium are better than in hydrogen or deuterium.

C. Neon Injection - Increasing the low Z impurity content, of course, reverses the effects of discharge cleaning and reduces the tungsten radiation. This occurs either naturally, when the machine is dirty or when a leak opens up in the vacuum vessel, or artificially by pulsing in neon, as shown in Figure 7. Initially, the deuterium discharge has a very high level of tungsten radiation. Around the time $t \approx 200$ ms, neon is injected, the tungsten radiation drops by a factor 5, and the central electron temperature increases from 900 eV to 2000 eV.

Discharges with low-Z contamination show the highest electron temperature (up to at least 2.5 keV). However, the density is limited by disruptions to relatively low values.

III. Energy Confinement

Measurement of the increase in temperature of the limiter after a plasma shot shows that only a small fraction (5-10%) of the total ohmic heating input is deposited on the limiter. Bolometer measurements indicate that 70-90% of the power input goes to the wall as radiation (including a small contribution by charge exchange neutrals). The difference, 5-30%, may represent charged particle transport to the vacuum vessel wall but is within the probable error of the measurements. The predominance of radiation losses distinguishes PLT from our earlier tokamaks.

For the energy balance within the plasma, we encounter two situations. In the first case, the local ohmic heating power input is almost balanced by radiation loss. This occurs in discharges with strong tungsten radiation (Type I and II). The energy balance in a hollow discharge is shown in Figure 8a. The curves for power input and radiation track each other closely (lower left). Plasma transport plays a minor role in the overall energy balance.

When tungsten radiation is small relative to power input (Type III, IV, V), plasma heat transport plays a larger role, particularly in the central region (Figure 8b). At larger radii near the limiter, radiation loss catches up with the power input. This outer radiation zone represents a virtual limiter[10], a highly desirable feature for protecting the physical limiter.

"Gross" confinement times, τ_E', that is total energy content (ion plus electron) divided by total ohmic heating power, are shown in Figures 9 and 10. Figure 9 refers to discharges before TDC, and Figure 10 to recent TDC-cleaned helium discharges. The best confinement times are around 70 ms, and we tentatively conclude that they follow the familiar $n_e a^2$ scaling.

In order to obtain a true measure of energy transport through the plasma, some account must be taken of radiation. All the discharges of Figures 9 and 10 were optimized for confinement time (i.e., those of Types III, IV, V), and the radiation from the central core in those cases is typically 20-50% of the input power. The range is due partly to changes in discharge conditions, but also reflects a systematic tendency of the bolometric measurements to give higher loss rates than VUV spectroscopy. In these cases, then, the "transport confinement time," $W_{tot}/P_{in}-P_{rad})$, is at least 20% higher than the "gross" confinement time, or $\gtrsim$ 85 ms in the best cases. A systematic analysis of local energy transport in a variety of discharges is still in a preliminary stage.

For the investigation of the ion heat transport, the ion temperature was measured with charge exchange (using a neutral beam to enhance the neutral density in the center), with neutrons, and from the Doppler broadening of impurity lines. A typical radial profile of the ion temperature in a peaked sawtooth discharge (Type III) is shown in Figure 11. A detailed investigation of the ion energy balance, following Stott[11], shows that neoclassical heat conduction is the dominant process in determining the radial ion temperature profile. Charge exchange losses must be low because of the low neutral density in PLT. Some details are given in Figure 11 (lower right). In hollow discharges, the central ion temperature actually exceeds the electron temperature, because of the ion heat transport into the hollow region.

Summary

Low-temperature discharge cleaning has been used successfully on PLT to reduce the amount of oxygen (the primary low Z impurity in the discharge). With this reduction of low Z impurity concentration, the highest electron density is $\langle n_e \rangle \sim 10^{14}\ cm^{-3}$, and longest "gross" energy confinement time is $\tau_E \sim 70$ msec yielding a "transport" confinement time ≥ 85 ms. The effective ion charge, Z, has been reduced, but larger values of density and confinement time have not yet been achieved in D_2 discharges, and to only a slight extent in helium discharges. Gas injection programming must be used to obtain these good values; otherwise large amounts of tungsten radiation can overwhelm the discharge, causing it to develop a hole in the radial electron temperature profile; the associated confinement time can then be very low (~5 msec). It appears likely that edge cooling of the plasma is the mechanism that inhibits the influx of tungsten and makes possible the development of discharges with 70 msec confinement.

ACKNOWLEDGMENTS

The continuing support of Drs. M. B. Gottlieb and H. P. Furth is gratefully acknowledged. These experiments were carried out with the excellent technical assistance of M. Perron and his crew and the fine support of the computer group under F. Seibel.

This work was supported by U. S. Department of Energy, Contract EY-76-C-02-3073.

REFERENCES

[1]D. Grove, et al., Plasma Physics and Controlled Nuclear Research, Berchtesgaden, 1976 (Vienna, International Atomic Energy Agency, 1977), Vol 1, p. 21.

[2]R. J. Taylor and L. Oren, UCLA Report, PPG-294 UCLA (1977).

[3]E. Hinnov, et al., Bull. American Physical Society, 21, 1159 (1976).

[4]R. G. Burkhalter, et al., Naval Research Laboratory Report, NRL-3444 (1977).

[5]R. C. Isler, et al., Phys. Lett. (to be published).

[6]R. D. Cowan, Los Alamos Sci. Lab. Report, LA-6679-MS (1977)

[7]R. V. Jensen, et al., Princeton Plasma Physics Laboratory, PPPL-1334 (March, 1977).

[8]G. M. McCracken, private communication.

[9]H. P. Furth, et al., Phys. Fluids 13, 3020 (1970).

[10]W. Stodiek, 5th European Conference on Controlled Fusion and Plasma Physics, (Grenoble, Centre d'Etudes Nucleaires, 1972) Vol. 2, p. 1.

[11]P. E. Stott, Plasma Physics 18, 251 (April, 1976).

Table I

Gas	Helium	Deuterium	Hydrogen	Helium	Deuterium
Discharge Cleaning	PDC	PDC	TDC	TDC	TDC
Date	9/28-29/76	10/5/76	2/10-11/77	3/2/77	5/4/77
$\frac{n_{oxygen}}{n_e}$ *)	1.5%	7.5%	0.5%	0.5%	1.0%
$\frac{n_{carbon}}{n_e}$ *)	1.8%	1.2%	0.4%	0.4%	0.7%
Z_{eff} *)	3.2	5.6	1.4	2.3	1.6

*Spectroscopic measurements during the initial stages of discharge. Later in the discharge, the Z_{eff} from the influx was usually somewhat higher.

Table 2

	I Hollow Discharge	II Peaked m=2 Discharge	III Sawtooth Discharge With Gas Programming	IV High Density Helium	V Discharge With Low Z Contamination
1. Working Gas	H_2, D_2, He	H_2, D_2, He	H_2, D_2	He	H_2 + [illegible] H_2 + He
2. Discharge Cleaning	TDC	TDC PDC	[illegible]	[illegible]	[illegible]
3. $T_e(0)$ (keV)	[illegible] $T_{e\,max}$ [illegible]	[illegible]	[illegible]	[illegible]	[illegible]
4. $T_e(r)$	Hollow	Peaked Intermittent	Peaked	Peaked	Peaked
5. $n(0)$ (10^{13} cm^{-3})	3-4	[illegible]	[illegible]	[illegible]	[illegible]
6. Z_{eff} (From Laser)	2.0-[illegible]	[illegible]	[illegible]		[illegible]
7. τ_{E_e} (ms)	<5	[illegible]	3		
8. Tungsten Radiation (USX) $W(0)$ (mW cm^{-3})	~500	[illegible]	4[illegible]	[illegible]	
9. Bolometer Radiation $W(0)$ (mW cm^{-3})	800	[illegible]	4[illegible]	[illegible]	[illegible]
10. Central Ohmic Power Input $W_{OH}(0)$ (mW cm^{-3})	200 W_{max} ~1000	11[illegible]	1[illegible]		
11. $T_i(0)$ (Charge Exchange) (keV)	~0.5	[illegible]	[illegible]	[illegible]	
12. τ_{E_i} (ms)		[illegible]	[illegible]	[illegible]	
13. Fusion Neutrons (d-d) (sec^{-1})	$\leq 10^7$	[illegible]	[illegible]	---	[illegible]
14. MHD Instabilities From X-Rays	m=3 (m=2)	m=2	m=1 Sawtooth	m=1 Small Sawtooth	m=1 Large Sawtooth

Figure Captions

Fig. 1 Discharge cleaning in PLT. The partial pressure of water vapor is measured with the mass analyser during discharge cleaning and plotted against time. During the time intervals a, b, c..., indicated by arrows at the top of the graph, conditions were changed. The water vapor pressure is very high when TDC (time interval c and f) is applied and very low when PDC is used (time interval e).

Subfigure 1(a) and 1(b) show the water vapor reading between shots for TDC and PDC respectively. The TDC shot produces water, a PDC shot decreases water.

Fig. 2 Hollow radial profile of the electron temperature measured by Thomson scattering in a low density deuterium discharge. In the hollow region, power loss due to tungsten radiation exceeds ohmic heating power input. The Z_{eff} is relatively low, however. Discharge conditions: B_{TF} = 32 kG, I_{OH} = 360 kA, V_{OH} = 2.1 V, D_2, a = 40 cm, $\langle n \rangle$ = 2.6 10^{13}cm^{-3}, τ'_{E_e} = 8.65 ms, Z_{eff} = 2.3.

Fig. 3 VUV-spectrum in the 50 Å region, showing the tungsten bands centered around 33, 50, and 59 Å.

Fig. 4 Time development of a hollow deuterium discharge. (a) and (b) plasma electron temperature T_e and density n_e from Thomson scattering, (c) radiation in the 50 Å region from Abel inverted USX-data, (d) radiation in the 14 Å region from the USX detector. (The factors 1.9 and 3 on the ordinate are corrections for detector efficiency.)

Fig. 5 Time development of the tungsten radiation in a peaked deuterium discharge.

Fig. 6 Comparison of the 50 Å radiation in a hollow deuterium discharge (Type I) and a sawtooth discharge with gas programming (Type III). The late rise of the tungsten radiation in the deuterium discharge was avoided in high density helium discharges.

Fig. 7 Effect of injecting neon into a deuterium discharge at ~200 ms. The 50 Å tungsten radiation decreases strongly as neon enters the discharge (bottom). The electron temperature rises rapidly in the center and cools somewhat on the outside of the plasma column (top).

Fig. 8 Internal energy balance for a hollow deuterium discharge (a), and neon discharge (b). Plotted are (top) power input and radiation loss per cm^3 vs radius, and (bottom) the volume integrals over these quantities up to radius r.

Fig. 9 Energy confinement time vs $n_e a^2$ where n_e is the average density and a is the limiter radius.

Fig. 10 Energy confinement time vs density for high density helium discharges.

Fig. 11 Ion energy balance. The ion temperature profile was measured with charge exchange ■, neutrons ▲, and Doppler broadening ο (lower left). The ion temperature is calculated with a computer code (shaded area), using Thomson scattering electron temperatures and a neutral gas diffusion code, incorporating electron ion coupling (Q_{ei}), neoclassical thermal conduction (Q_{TC}), particle diffusion (Q_{PD}), charge exchange (Q_{CX}) and electron ionization (Q_{IZ}) (lower right). Plotted also are the ion energy confinement time, τ_{Ei} (top left), the neoclassical heat conductivity K_i (top right), and the collisionality parameter $\nu^*/\epsilon^{3/2}$ (top right).

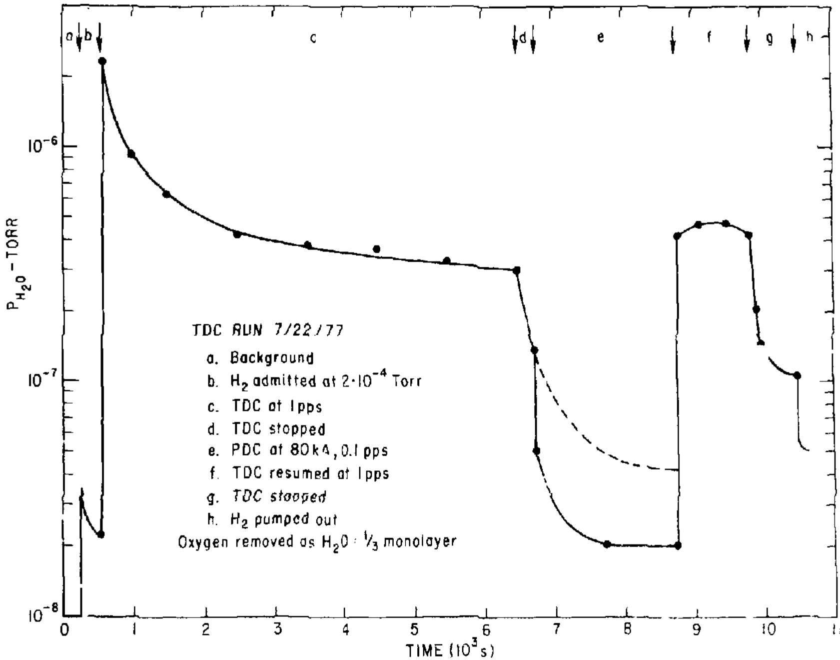

a
b
c
d
e
f
g
h
TDC RUN 7/22/77
a. Background
b. H_2 admitted at $2 \cdot 10^{-4}$ Torr
c. TDC at 1pps
d. TDC stopped
e. PDC at 80kA, 0.1 pps
f. TDC resumed at 1pps
g. TDC stopped
h. H_2 pumped out
Oxygen removed as H_2O ≈ 1/3 monolayer
P_{H_2O} - TORR
10^{-6}
10^{-7}
10^{-8}
0
1
2
3
4
5
6
7
8
9
10
11
TIME (10^3 s)

Fig. 1. 773869

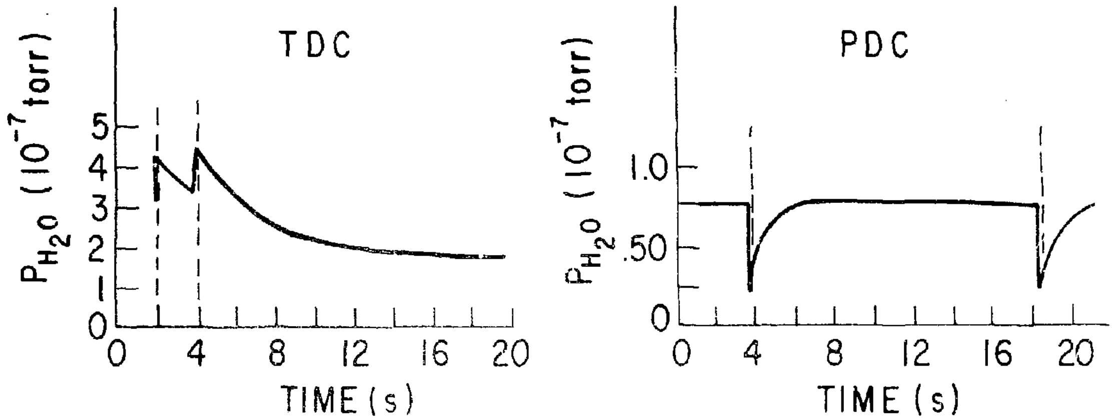

Fig. 1a & 1b. 773881

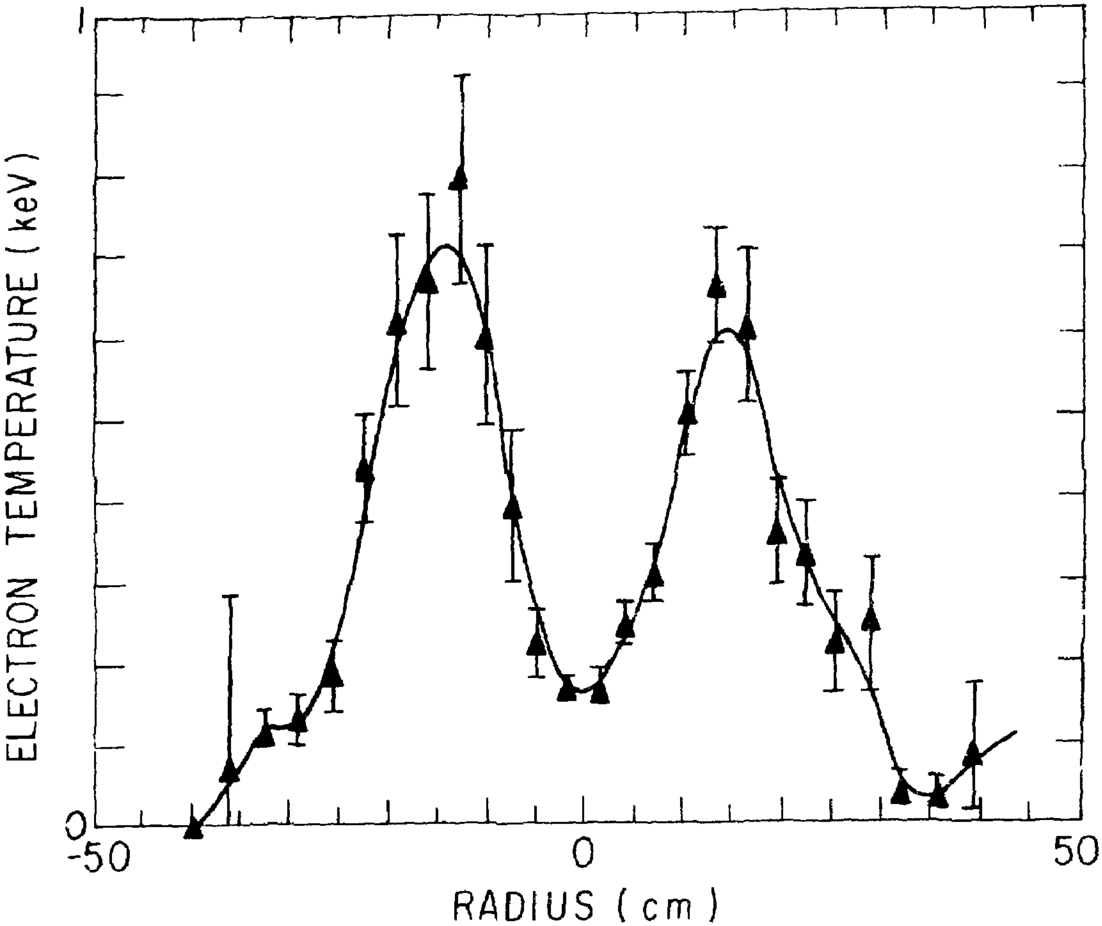

Fig. 2. 783295

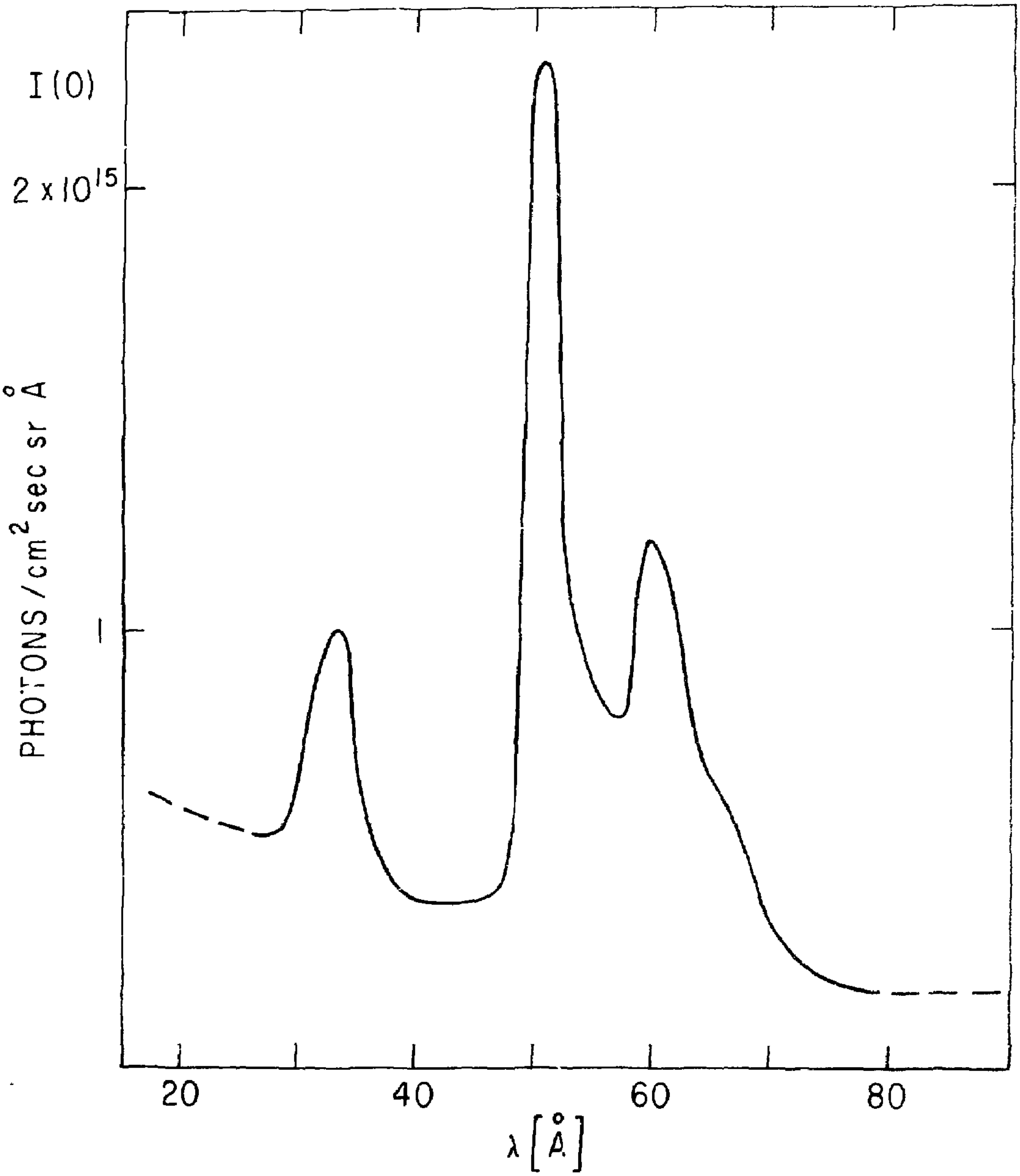

Fig. 3. 773504

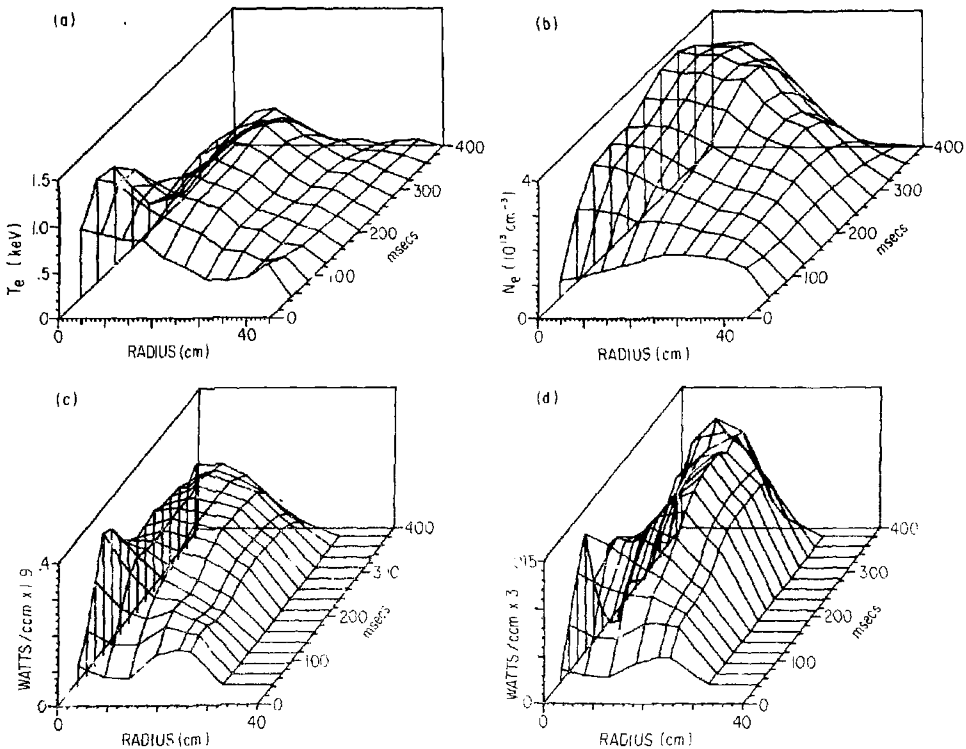
(a)
T_e (keV)
0
.5
1.0
1.5
RADIUS (cm)
40
msecs
100
200
300
400
(b)
N_e (10^{13} cm^{-3})
4
RADIUS (cm)
(c)
WATTS/ccm x 1 9
.4
(d)
WATTS/ccm x 3

Fig. 4. 773851

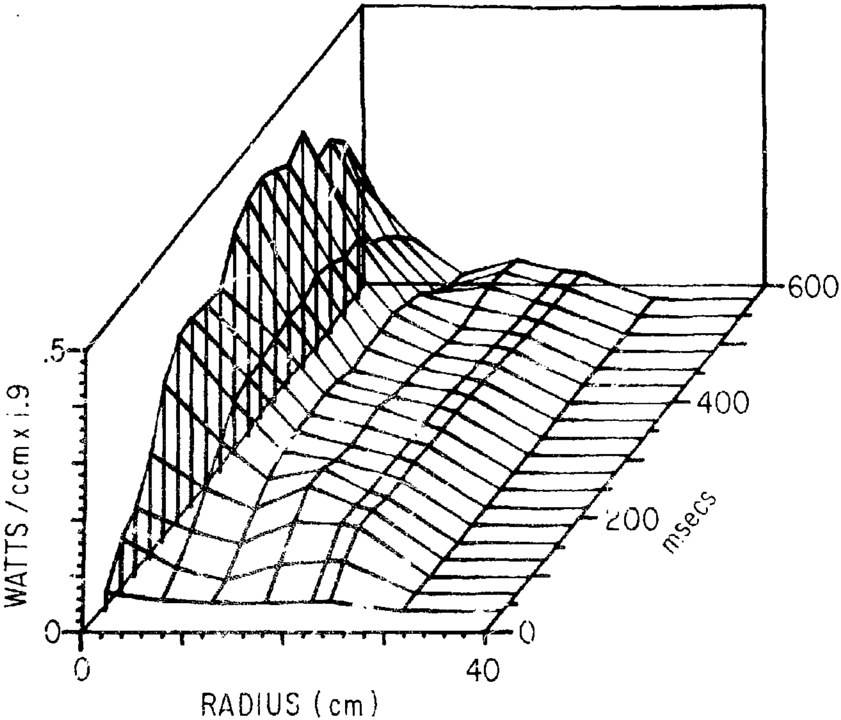

Fig. 5. 773784

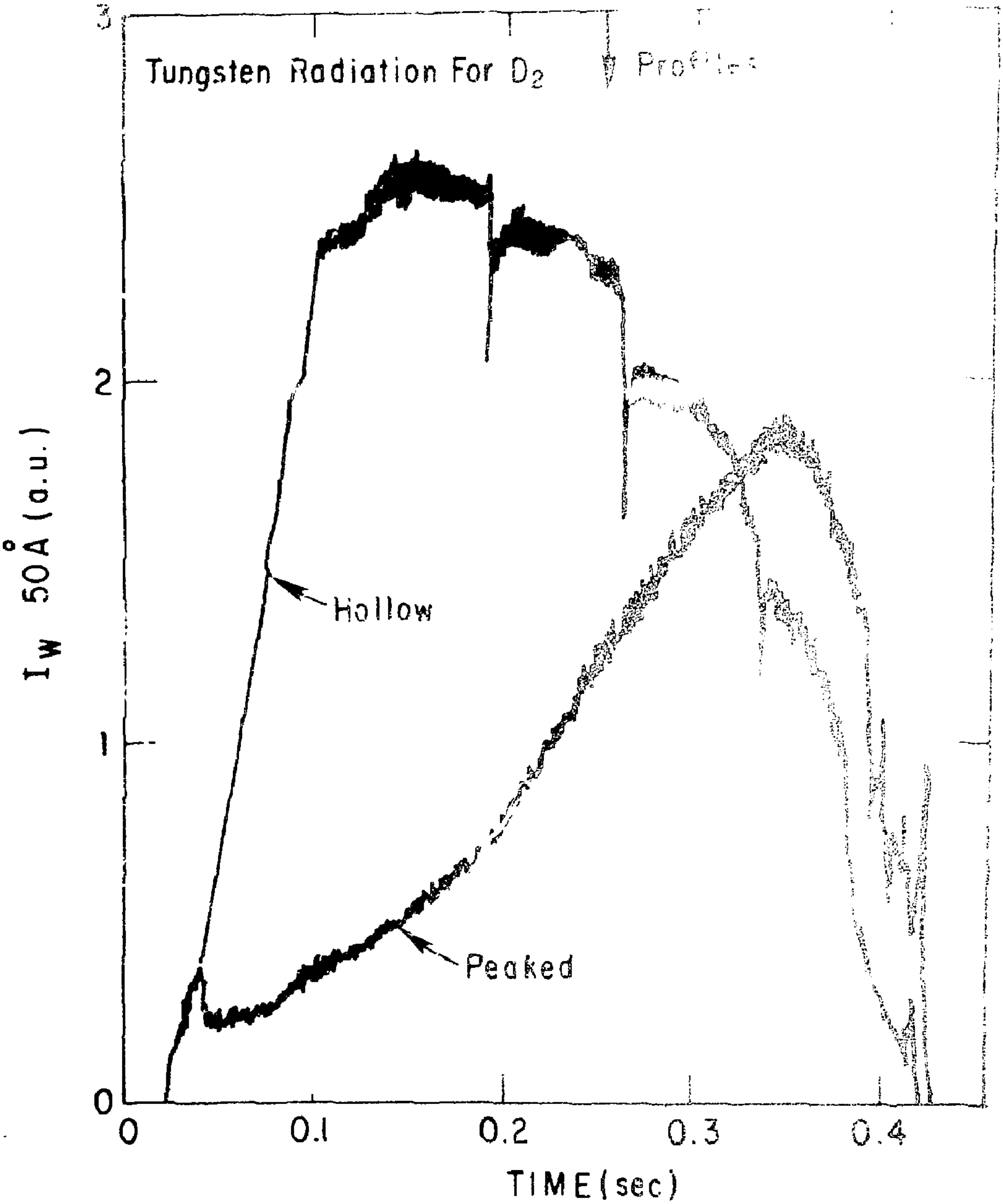

Tungsten Radiation For D_2
Profiles
Hollow
Peaked
I_W 50Å (a.u.)
TIME (sec)
0
1
2
3
0.1
0.2
0.3
0.4

Fig. 6. 773865

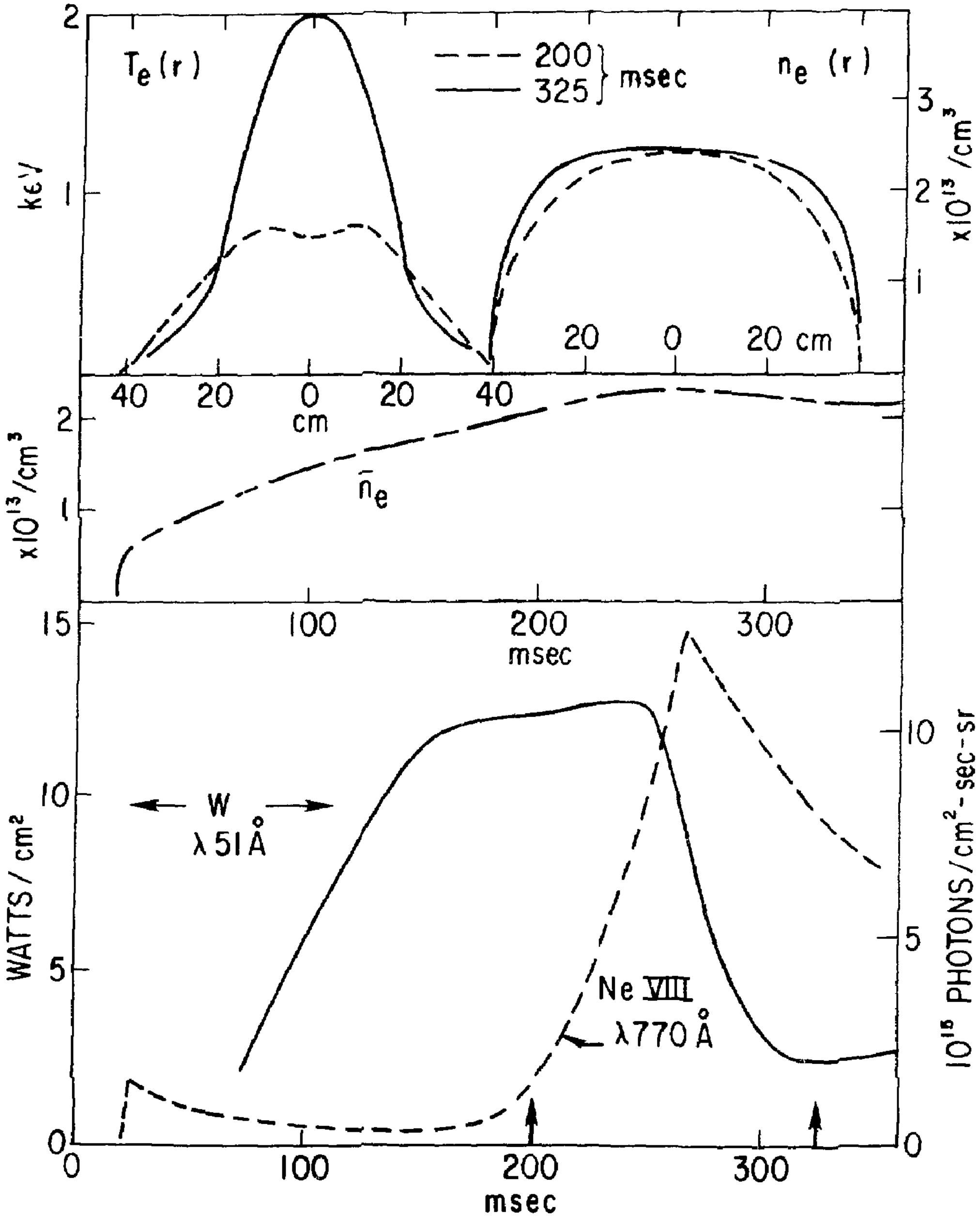

2
1
keV
$T_e(r)$
200
325
msec
n_e (r)
3
2
1
x10¹³ /cm³
20
0
20 cm
40
20
0
20
40
cm
2
1
x10¹³/cm³
$\bar{n}_e$
15
100
200
300
msec
10
5
0
WATTS / cm²
W
λ 51 Å
Ne VIII
λ770 Å
10
5
0
10¹⁵ PHOTONS/cm²-sec-sr
0
100
200
300
msec

Fig. 7. 773675

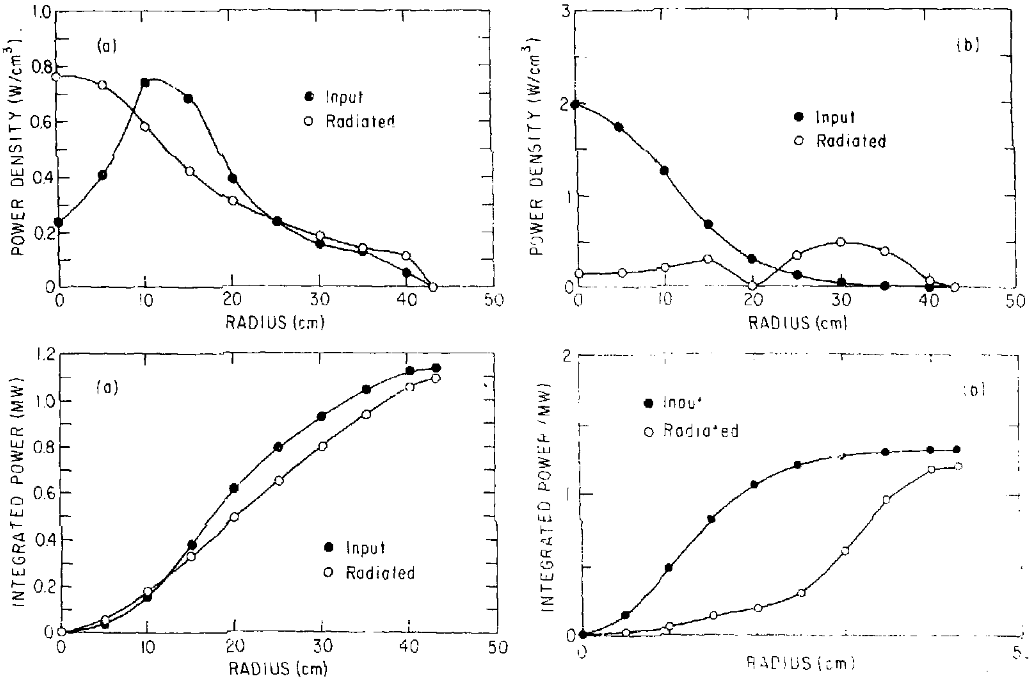

(a)
● Input
○ Radiated
POWER DENSITY (W/cm³)
RADIUS (cm)
(b)
INTEGRATED POWER (MW)

Fig. 8. 783296

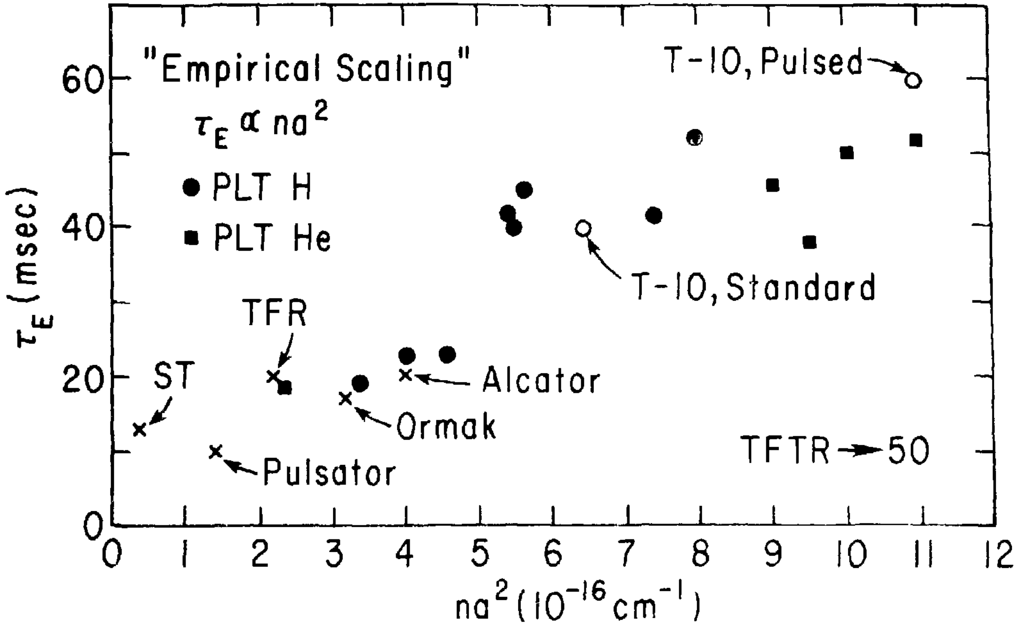
"Empirical Scaling"
$\tau_E \propto na^2$
PLT H
PLT He
T-10, Pulsed
T-10, Standard
TFR
ST
Alcator
Ormak
Pulsator
TFTR → 50
τ_E (msec)
na^2 (10^{-16} cm^{-1})
0
20
40
60
0
1
2
3
4
5
6
7
8
9
10
11
12

Fig. 9. 783306

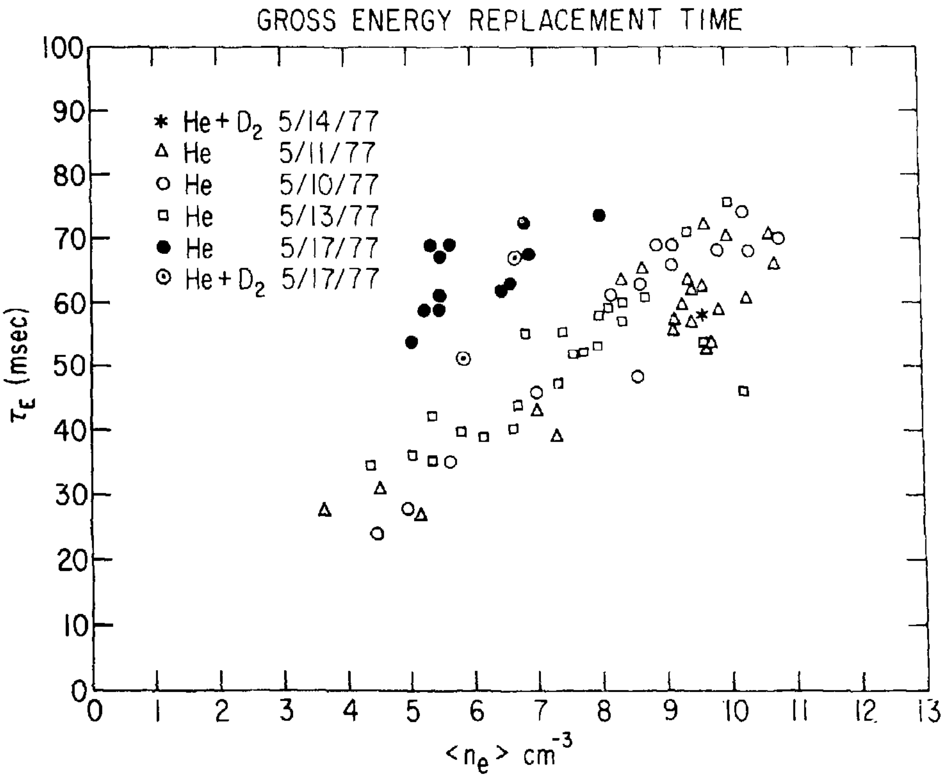

Fig. 10. 773393

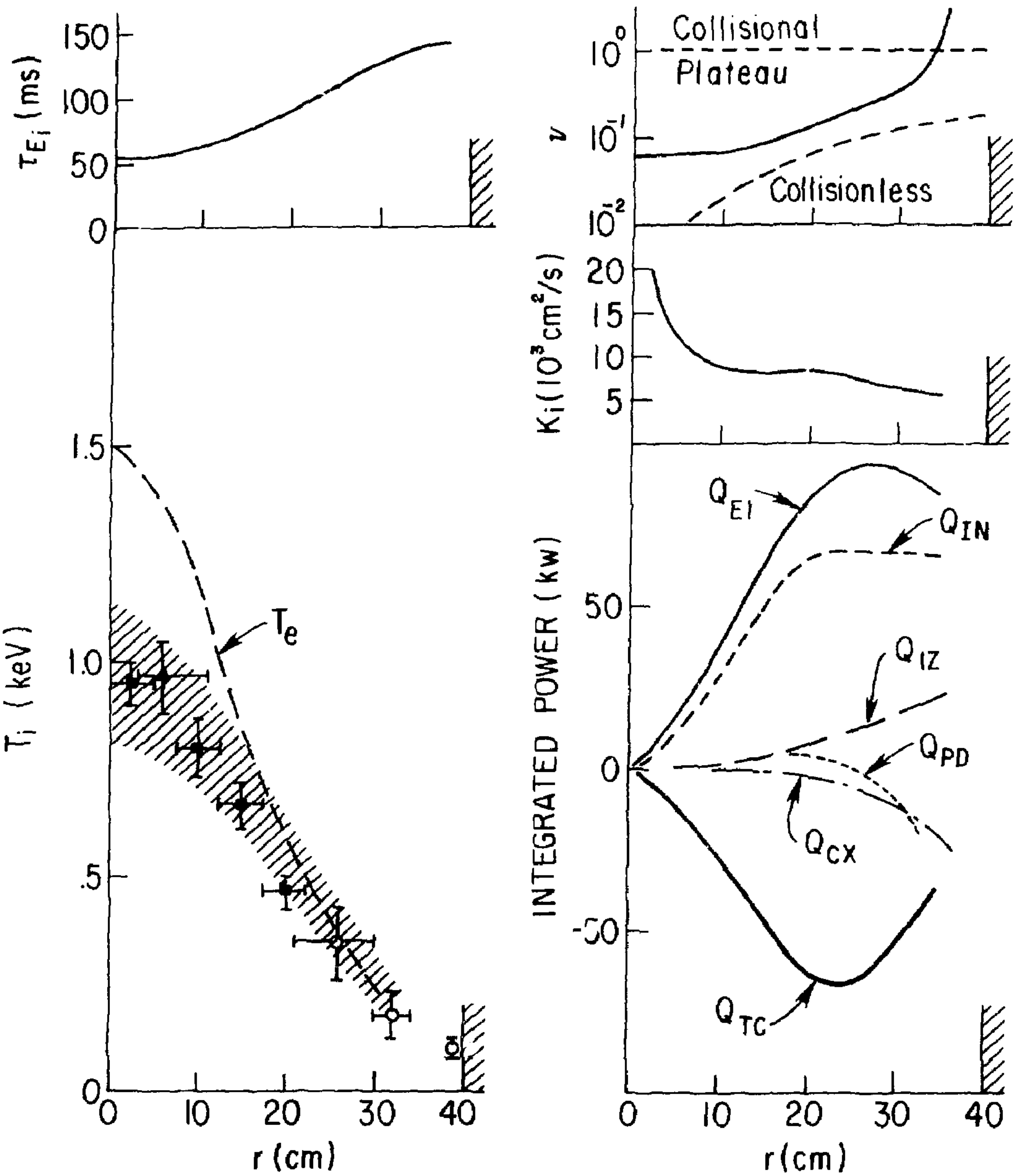

Fig. 11. 776C57